* Manuscript

A METHOD FOR EVALUATING THE MECHANICAL PERFORMANCE OF THIN-WALLED TITANIUM TUBES

P.M. MacKenzie, C.A. Walker, J. McKelvie

Department of Mechanical Engineering,

University of Strathclyde,

Glasgow G1 1XJ,

Scotland, UK .

peter.mackenzie@strath.ac.uk

Tel: 0141 548 2045

Fax: 0141 552 5105

ABSTRACT

A method which was developed to compare the stress-strain properties of three types of thin-walled, commercially pure titanium tubes is presented. The tubes were of types intended for use in large heat-exchanger applications and were to be subjected to significant plastic deformation during subsequent assembly processes. It had been anticipated that small differences in chemical composition and tube-drawing treatment would produce quite different characteristics. It is known that the properties of titanium can exhibit considerable degrees of anisotropy, especially for wrought products; although axial properties of the materials could be evaluated using standard test equipment and procedures, a novel testing system had to be designed to allow the circumferential properties to be assessed. Significant differences between tube types were observed and anisotropic material behaviour was apparent.

Keywords:- anisotropic; commercially pure titanium; ductility; mechanical testing; hydraulic; tubes.

INTRODUCTION

Titanium and its alloys have desirable blends of properties such as low density, high strength and high stiffness, each of which makes them attractive for many structural applications. Coupled to these benefits are exceptional levels of resistance to corrosion and oxidation and, compared with aluminium alloys, distinctly better creep-resistance. For these reasons, the use of titanium and its alloys can be justified economically in an increasing range of high-integrity areas, from aerospace to petrochemicals (and not forgetting to mention the growing market in sports goods).

Approximately 25% of the market for metallic titanium is made up of the commercially pure (CP) form. CP titanium is, in effect, an alloy of titanium, oxygen and traces of several other elements. Although, in all of the various varieties which come under the CP designation, metallic titanium makes up in excess of 99% of the content, the small fractions of other elements which may be included can influence the mechanical properties to a very significant degree. Most notably, small, controlled amounts of oxygen are dissolved in solid solution to produce increases in strength but, ultimately, with a significant reduction in ductility. CP titanium generally displays good ductility and can be forged, rolled, drawn or extruded quite straightforwardly but its hexagonal close packed (α–phase) structure does limit formability. In addition, the textures developed in wrought products for α– titanium and its alloys can have a marked effect on the mechanical properties of the finished material and distinctly anisotropic material behaviour can be a common feature **[1 - 6].**

The work presented here was focussed on evaluating mechanical properties of thin-walled CP titanium tubes intended for use in heat exchangers. The key justification of the work was that, during the fabrication process, expansion of tubes into tube-sheets produces high levels of plastic deformation of the tube material circumferentially **[7,8]** and, to this end in particular, a novel method for assessing the response of the material in the circumferential direction was required.

SPECIMEN MATERIALS

Specimens of three different types of drawn tube were used in the investigation. Details of oxygen content together with tube dimensions are summarised in Table 1.

Figure 1 contains representative micrographs of the grain structure of each of the three specimen groups, designated Types ‘A’, ‘B’ and ‘C’. Type ‘A’, the only vacuum annealed sample, shows very much larger grain diameter (by a factor of 4 to 5 approximately **[9]**) than do either of the other types. The three dimensional nature of the texture could not be assessed by optical microscopy alone and was beyond the scope of the present work.

AXIAL AND CIRCUMFERENTIAL LOADING CONFIGURATIONS

Axial testing of the tubes was performed in a relatively straightforward manner, as prescribed in **[10],** the British Standard**.** This requires quite simply that the tube ends, through which loads were to be applied, be reinforced in a prescribed manner; it also places requirements on the rate of loading and the method of recording results (these are discussed below). Specimen tube lengths of 400 mm satisfied the requirement of the standard test. Loads were applied using an Instron 1342 servo-hydraulic test machine.

By contrast, an entirely novel setup had to be designed in order to enable circumferential loading of the material, with axial stresses, up to yield point at least, eliminated as far as possible; there is no published prior art with regard to this.. Whilst there is a wealth of literature relating to the contiguous technology of hydroforming, for example, **[11 - 14],** this almost invariably deals with the application of intentional biaxial loading conditions. Indeed, **[13]** describes a method of testing tubular specimens with deliberately induced biaxial loads, so as to simulate the conditions found in the hydroforming process. The hydraulic test rig constructed for the present purpose is shown schematically in Figure 2. It was designed to perform two main functions: to ensure loading of the specimens in the desired manner, i.e., no, or minimal, axial loading up to yield; and to enable controlled application of the loading or expansion, this being achieved by having the Instron test machine previously mentioned adapted to provide the driving force for the rig. As shown in Figure 3, the test rig was mounted between the platens of the test machine, thereby enabling full feedback control of the pressure applied to the specimens.

SPECIMEN SEALING ARRANGEMENTS

The test rig also incorporated the specimen holder consisting of a removable steel core, with seals, mounted between a crosshead and the pump body. Specimens of dimensions given in Figure 4 were mounted on the core, and through this, the pressurised hydraulic oil was delivered.

Initially, it had been intended that the specimen sealing arrangement would consist of a bespoke nitrile rubber bladder but this proved to be unsatisfactory. From axial test results, it had appeared that pressures of approximately 100 MPa might be required in order to take the tubes to failure. This system was capable of containing only 10% of the target value. Bonding the seal to the central core using cyanoacrylate adhesive produced a substantial improvement in performance but, at seal failure pressures of about 60 MPa, this still fell short of the programme requirement.

In order to minimise axial loads up to yield, it was essential that the tubes be free-floating, i.e., the ends could not be plugged during the tests. To this end, an alternative technology to the bladder seal proved to be entirely satisfactory. This consisted of a setup using conventional nitrile rubber 'O'-ring seals on a special core, in tandem with spiral PTFE backing washers to prevent seal extrusion (Figure 5). Steel rings of thickness 2mm and diameter 0.2mm greater than those of the specimens were used to support the specimen at the point of contact with the 'O'-rings. This setup allowed pressures up to 140 MPa to be contained.

A key feature of the design is that the pressure end-loads imparted through the specimen cores were supported by, on the one hand, the pump body, and on the other, by the retaining cross-head mounted on reaction columns. By using two-piece cores, a potential problem in the oil-way at the core to body seal was eliminated since it was possible, by selecting appropriate dimensions, to ensure that the outward hydraulic force tending to open the seal was always more than balanced by the pressure force on the core from within the specimen.

Prior to each test, the hydraulic system, including the fresh specimen, was recharged with working fluid (Esso Nuto-H46) by first evacuating it to ensure no air pockets remained.

TEST PROCEDURE

Instrumentation comprised: Instron 100kN load cell (for the axial loading configuration); Shape 140 MPa pressure transmitter (for the circumferential loading configuration); a purpose-built clip-gauge diametrical strain transducer, Figure 6, essentially, two spring steel blades to which were attached four 6.35mm 1000Ω strain gauges connected in full-bridge configuration; 6.35 mm 120Ω strain gauges for attachment directly to the specimens; signal conditioning electronics; autographic recording equipment.

The specimen strain gauges were used during the hydraulic tests to monitor more precisely the behaviour up to yield, the diametrical transducer being intended for measurement of gross strains only. The diametrical transducer was calibrated and checked for linearity using precision ground cylindrical gauge bars; in practice, it was found invariably to give readings within 0.5% of micrometer measurements of the specimen diameters at failure.

In evaluating the axially loaded properties of the tubes, a conventional setup was used. The loads were obtained from the test machine load cell and displacements to yield whilst a 50 mm gauge-length LVDT displacement transducer provided measurements of extension. Elongation at failure was measured using pre-marked scales on the specimens over an initial gauge-length of 50 mm.

Strain rates for both loading configurations were set to be in the range 50 to 120 microstrain per second up to the 0.2% proof stress level, followed by an increase in rate to give failure within one additional minute.

Figure 7 shows representative traces, taken from the circumferential loading tests, of internal pressure v. diametrical strain records for each of the three sample types.

RESULTS AND DISCUSSION

The results are summarised in Table 2, and in Figure 8. For the axial loading configuration, the values given are for engineering stress-strain and similarly for the circumferentially loaded case, except that here, instead of the tensile strength being given, the circumferential stress component at failure has been presented; this was calculated using the recorded internal pressure, P_f, and the final maximum internal radius, r_f, at failure, to obtain the applied circumferential stress thus:

$$\sigma_h = \frac{P_f r_f}{t} \quad \ldots\ldots\ldots\ldots\ldots\ldots\ldots\ldots\ldots\ldots (1)$$

The tensile strength for the axial case was taken, conventionally, to be the engineering stress taken from the maximum point on the load-displacement curve. The distinct yield point for the Type 'C' record shown in Figure 7 was, to a varying degree, apparent for all Type 'C' specimens tested.

There are some areas to be careful of in examining these data. First of all, whilst it is reasonable to use the results for axial elongation at failure to compare the performance of the different tube types, and to use, similarly, the diametrical strain results, to make direct comparison between the axial and diametrical strain performance would be unsound. The failure by necking in the axial-loading case produces a very different plastic flow regime from that observed in the circumferentially loaded tests. Furthermore, the gross changes in tube geometry observed in the circumferential loading tests progressively introduced an increasingly significant axial component of stress. In other words, the performance one is able to observe here is influenced by the specimen geometry at high strain levels; the test should be regarded as a method for assessing the material-component combination, not as a proposed standard material test *per se*. For hydraulic loading in the setup developed here, and by measuring the change in internal radius from the initial condition, r_1, to any strained (bulged) condition of radius, r_2, one can evaluate the magnitude of the axial hydraulic force. From this, the ratio of applied stress components is given by equation (2):

$$\frac{\sigma_{AXIAL}}{\sigma_{HOOP}} = \frac{P(r_2^2 - r_1^2)}{2r_2t} \cdot \frac{t}{Pr_2}$$

$$= 0.5 \cdot \left(1 - \left(\frac{r_1}{r_2}\right)^2\right)$$

$$= 0.5 \cdot \left(1 - \left(\frac{1}{1+\varepsilon_d}\right)^2\right) \quad \ldots\ldots\ldots\ldots\ldots\ (2)$$

Thus, for the maximum value of diametrical strain, ε_d, observed during hydraulic testing (69%), an axial component of stress equal to 32% of the applied circumferential stress would be induced. On the other hand, at the typical strain values (about 0.6%) measured at the Proof Stress, the axial component of stress introduced due to the bulging of the tubes can be shown to amount to much less than 1% of the applied circumferential stress.

We can note certain other points with a considerable degree of confidence, however. It is clear that, of the three batches, Type 'B', with the lowest oxygen content, exhibited the lowest Proof Stress, the lowest tensile strength, and the highest ductility for both loading configurations. Type 'C', having the highest oxygen content, also showed the highest values for both axial tensile strength and for failure pressure in the hydraulic tests, but with by far the greatest degree of scatter of the three tube types. Figure 9 shows two examples of circumferentially loaded Type 'C' tubes post-failure; of the thirteen specimens of this type, ten failed by pinhole leak and the remaining three by unstable fracture. In the cases where fracture occurred, the diametrical strain at failure was at the upper end of the range for this type (73 % to 77% for the three results, compared to a mean of 63%). All of the Type 'A' and Type 'B' specimens failed by unstable fracture.

Given the negligible change in geometry observed at the yield point, one can reasonably draw comparisons between the axial and circumferential values for Proof Stress: whilst Types 'B' and 'C' showed increases of 31% and 25% respectively in the circumferential direction, Type ‘A’ the large-grained vacuum annealed batch, proved to be closer to isotropic in this respect showing an increase of only 14%.

In passing, it might be noted that the Hall-Petch relationship **[15, 16]** states that:

$$\sigma_y = \sigma_0 + \frac{K}{\sqrt{d}} \quad \ldots\ldots\ldots\ldots\ldots\ldots\ldots (3)$$

where the yield stress, σ_y, can be predicted as a function of: σ_0, the “intrinsic yield” of the material; d, the grain diameter; and K, a material constant. In the present case, although the three sets of specimens were of near identical chemical composition (and within the range prescribed for “commercially pure”), a cursory inspection of the micrographs in Figure 1 confirms that Type ‘B’ has the smallest grain size and yet it also has the lowest measured values of σ_y for both axial and circumferential loading cases. In other words, the observed results run counter to the relationship and it therefore does not hold for this situation. This can be explained in that, as previously stated, the mechanical properties of CP titanium are highly sensitive to very small variations in chemical composition (of the scale seen here) and, furthermore, an additional determining factor, the initial level of dislocation density in the materials was “as manufactured”, i.e., was not deliberately controlled for investigative purposes.

In summary, the primary objective of this work was to devise a system to enable objective evaluation of, and comparison between, the properties to failure for tube specimens of near-identical geometry and the results obtained from the test setup which was developed have demonstrated its capability of performing this task satisfactorily.

CONCLUSIONS

A system for making comparative evaluations of, separately, the axially and circumferentially loaded performance of tubular specimens of CP titanium has been demonstrated. This required the development of a new experimental setup for applying circumferential stresses hydraulically; using this, axial loads were essentially eliminated up to specimen yield. The arrangement also enabled useful comparisons to be made of ductility up to failure with circumferential loading predominant. Axial load testing followed the prescribed method of a standard test procedure.

Tests were performed on three candidate tube types intended for a large-scale heat exchanger application. Measured mechanical properties differed significantly between the three types. All three batches displayed yield behaviour which to a significant degree was dependent on orientation. Differences in performance between the tube types could not be attributed directly to observed differences in average grain size. The tests confirmed that tube Type 'C', having the highest oxygen content, was, generally, the strongest of the three groups over both loading regimes, but at little or no cost in relation to its ductility; Type 'C' was, therefore, deemed most appropriate for the proposed high-integrity application.

Finally, the findings confirm that, where it is a requirement that detailed quantitative comparison be made between types of CP titanium tube produced by different manufacturing process, or having small differences in chemical composition, it is important to conduct tests on specimens of finished tubes, there being no convenient method available for reliably inferring mechanical properties otherwise.

REFERENCES

1) Titanium Information Group, *Titanium for Marine and Offshore Applications – A Designers' and Users' Handbook.* Kjeller, Norway: Institutt for Energiteknikk, 1999.

2) Seagle, S.R., The state of the USA titanium industry in 1995. *Materials Science and Engineering* 1996; A213, 1–7.

3) Yamada, M., An overview on the development of titanium alloys for non-aerospace application in Japan, *Materials Science and Engineering* 1996; A213, 8–15.

4) Jaffee, R.I., Promisel, NE., (eds), *The Science, Technology and Application of Titanium*. Oxford, UK: Pergamon Press, 1970.

5) Bache, M.R., Evans, W.J., Suddell, B., Herrouin, F.R.M., The effects of texture in titanium alloys for engineering components under fatigue, *International Journal of Fatigue* 2001; 23, S153 – S159.

6) Davies, R.W., Khaleel, M.A., Kinsel, W.C., Zbib, H.M. (2002) Anisotropic yield locus evolution during cold pilgering of titanium alloy tubing, *Trans ASME, Journal of Engineering Materials and Technology* 2002; 124, 125 – 134.

7) Goodier, J.N., Schoessow, G.J., The holding power and hydraulic tightness of expanded tube joints: analysis of the stress and deformation, *Trans ASME* 1943; 65, 489-96.

8) Alexander, J.M, Ford, H., On Expanding a Hole from Zero Radius in a Thin Infinite Plate, *Proceedings of the Royal Society of London. Series A, Mathematical and Physical Sciences* 1954; 226, 543-561.

9) ASTM, *Standard test methods for determining average grain size, E112-96*, 1996.

10) BS EN 10002 - 1:2001, *Metallic materials – tensile testing*, British Standards

Institute, 2001.

11) Tirosh, J., Neuberger, A., Shirizly, A., On tube expansion by internal fluid pressure with additional compressive stress, *International Journal of Mechanical Science* 1996; 38, 839-851.

12) Zhang, S.H., Developments in hydroforming, *Journal of Materials Processing Technology* 1999; 91, 236-244.

13) Sokolowski, T., Gerke, K., Ahmetoglu, M., Altan, T., Evaluation of tube formability and material characteristics: hydraulic bulge testing of tubes, *Journal of Materials Processing Technology* 2000; 98, 34-40.

14) Lang, L.H., Wang, Z.R., Kang, D.C., Yuan, S.J., Zhang, S.H., Danckert, J., Nielsen, K.B., Hydroforming highlights: sheet hydroforming and tube hydroforming, *Journal of Materials Processing Technology* 2004; 151, 165-177

15) Polmear, I.J. (1989) *Light Alloys*. London, UK: Edward Arnold, 1989.

16) Kao, Y.L., Tu, G.C., Huang, C.A., Liu, T.T., A study on the hardness variation of α- and β-pure titanium with different grain sizes, *Materials Science and Engineering* 2005; A 398, 93-98.

FIGURES AND CAPTIONS

FIGURE 1: Micrographs of Type 'A', 'B' and 'C' commercially pure titanium tube specimens.

FIGURE 2: Schematic of self-contained high-pressure pump and specimen holder.

FIGURE 3: Pump and specimen holder mounted in jaws of servo-hydraulic test machine.

FIGURE 4: Specimen dimensions.

FIGURE 5: Test-rig core and specimen sealing arrangement incorporating nitrile 'O'-rings and PTFE spiral backing washers to prevent seal extrusion.

FIGURE 6: Clip gauge diametrical strain transducer (dimensions in mm). 1000Ω strain gauges were positioned at 'SG'. The tube diameters were measure between the 38 mm radius arcs of a pair of jaws attached to the blade ends.

FIGURE 7: Sample records of applied internal pressure v. diametrical strain from circumferential loading tests.

FIGURE 7: Summary of results of tests to failure

FIGURE 8: Examples of post-failure Type 'C' specimens – unstable fracture and "pinhole" failure.

Figure1
Click here to download high resolution image

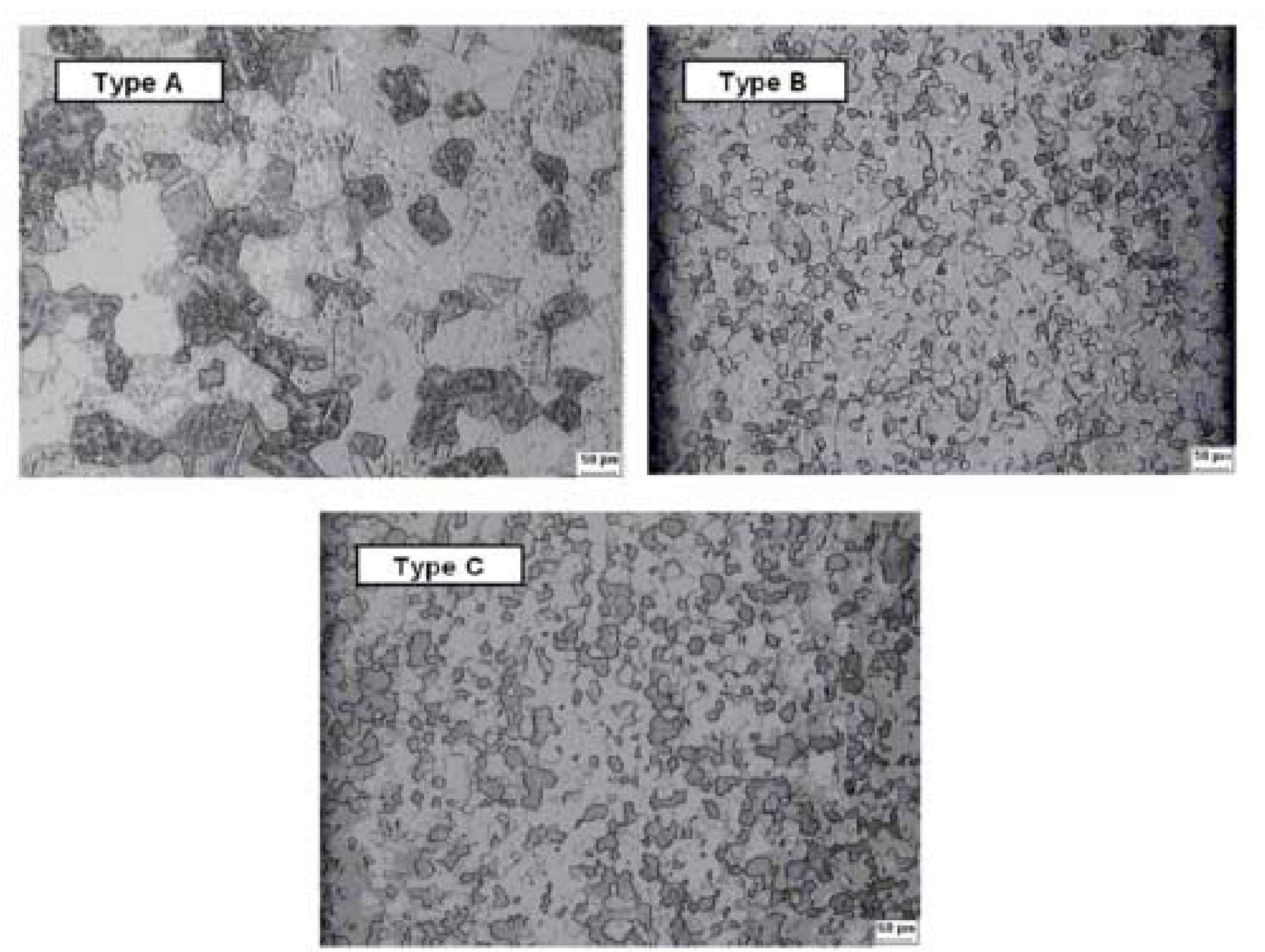

Figure2
Click here to download high resolution image

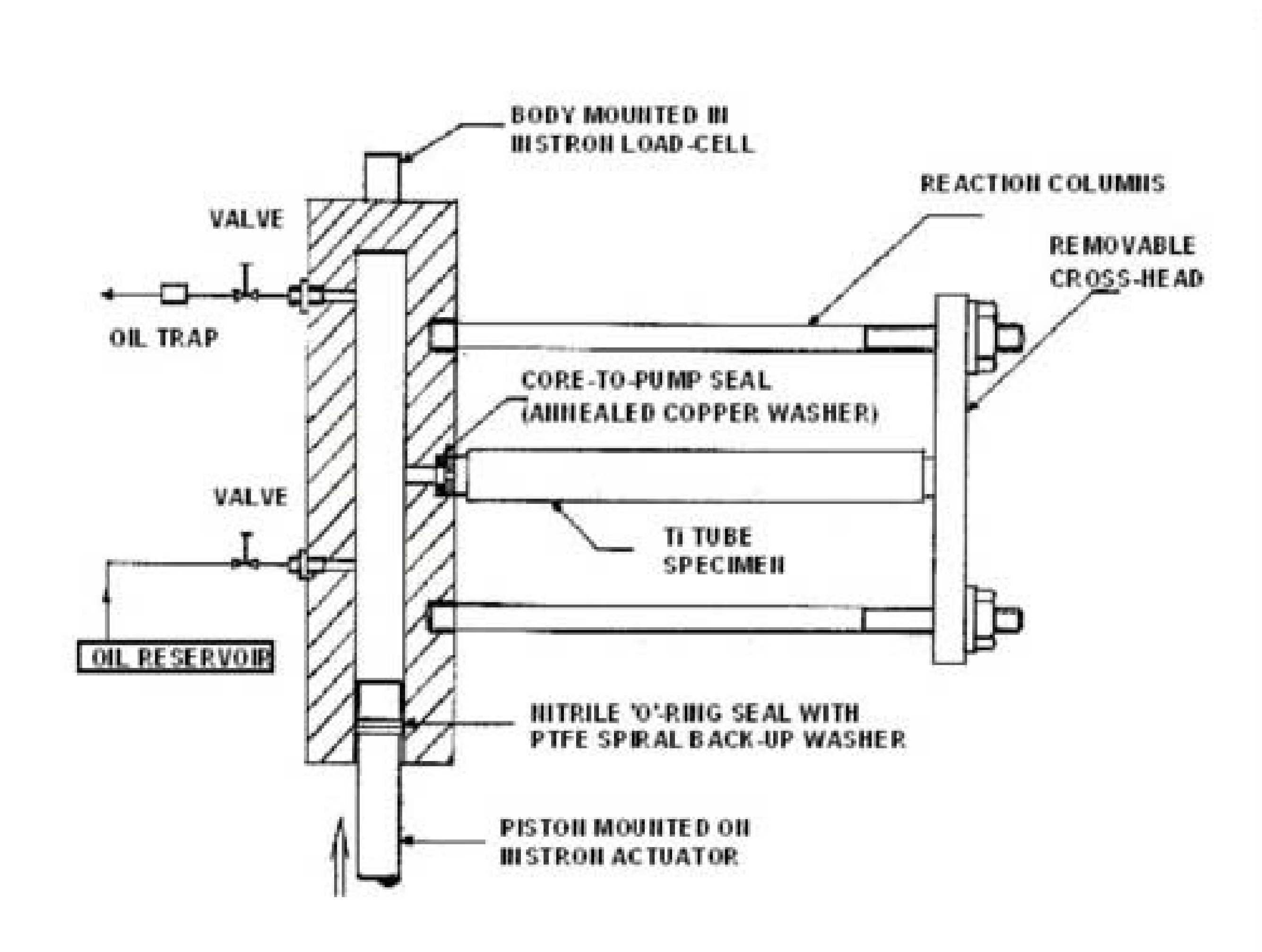

Figure3
Click here to download high resolution image

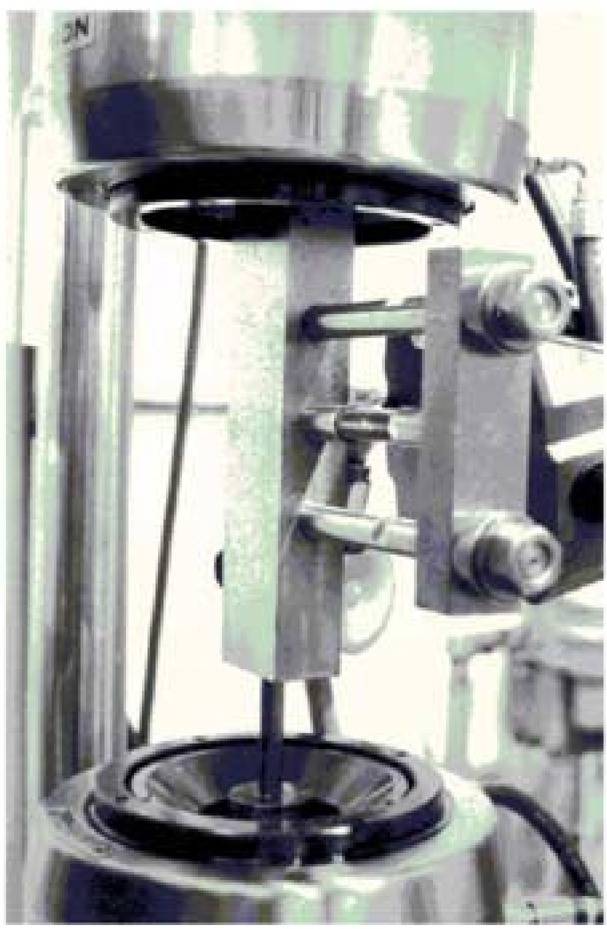

Figure4

Click here to download high resolution image

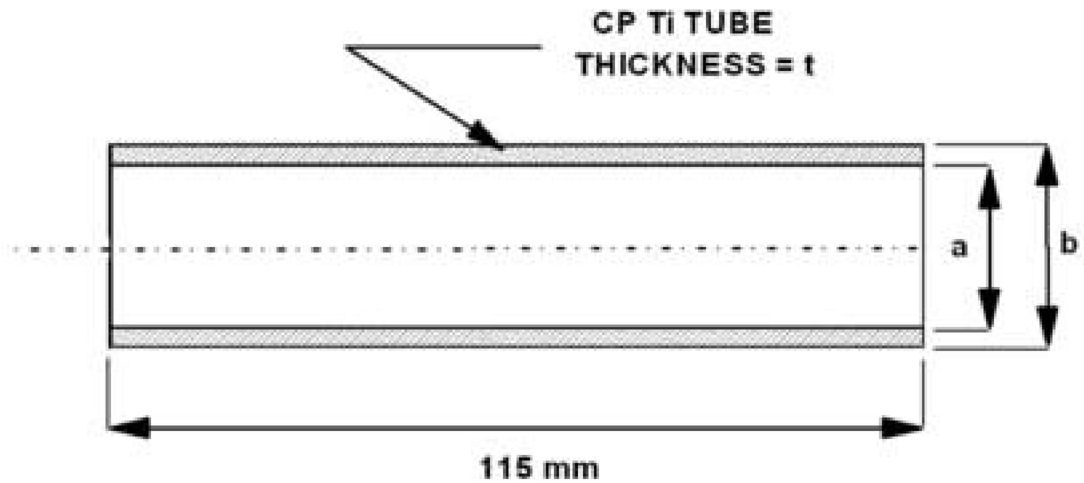

Figure5
Click here to download high resolution image

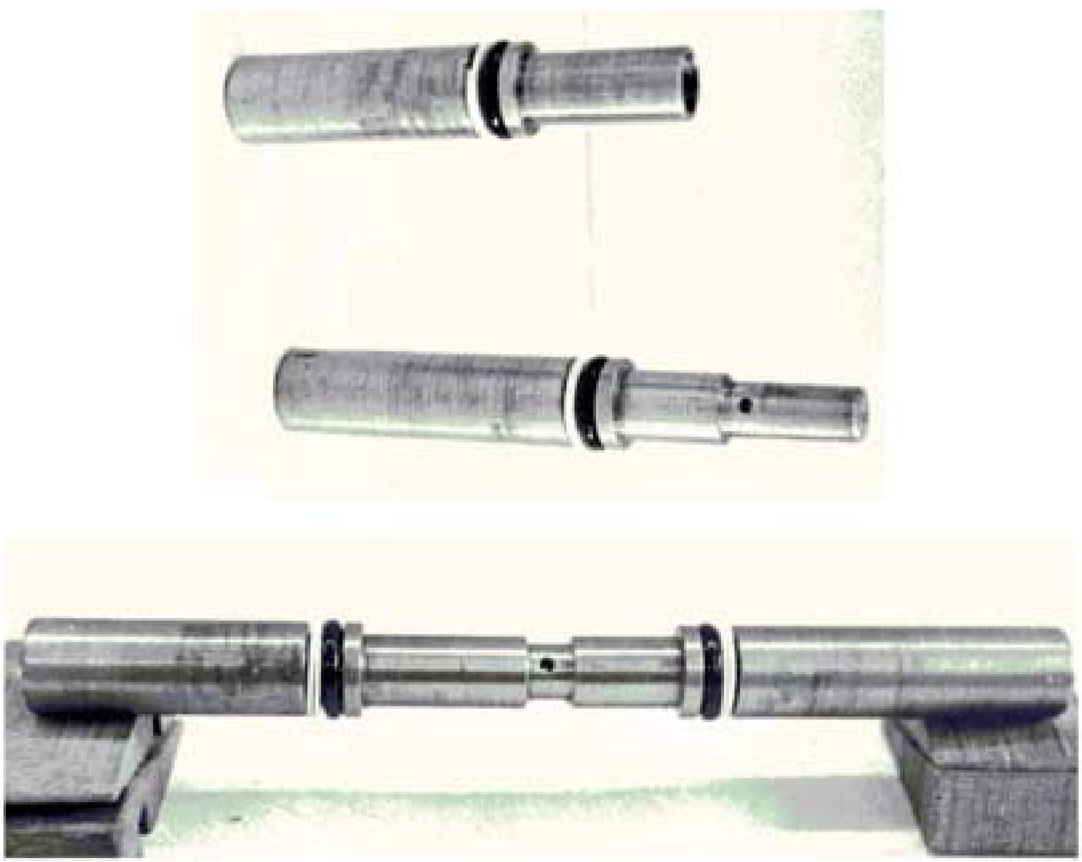

Figure6
Click here to download high resolution image

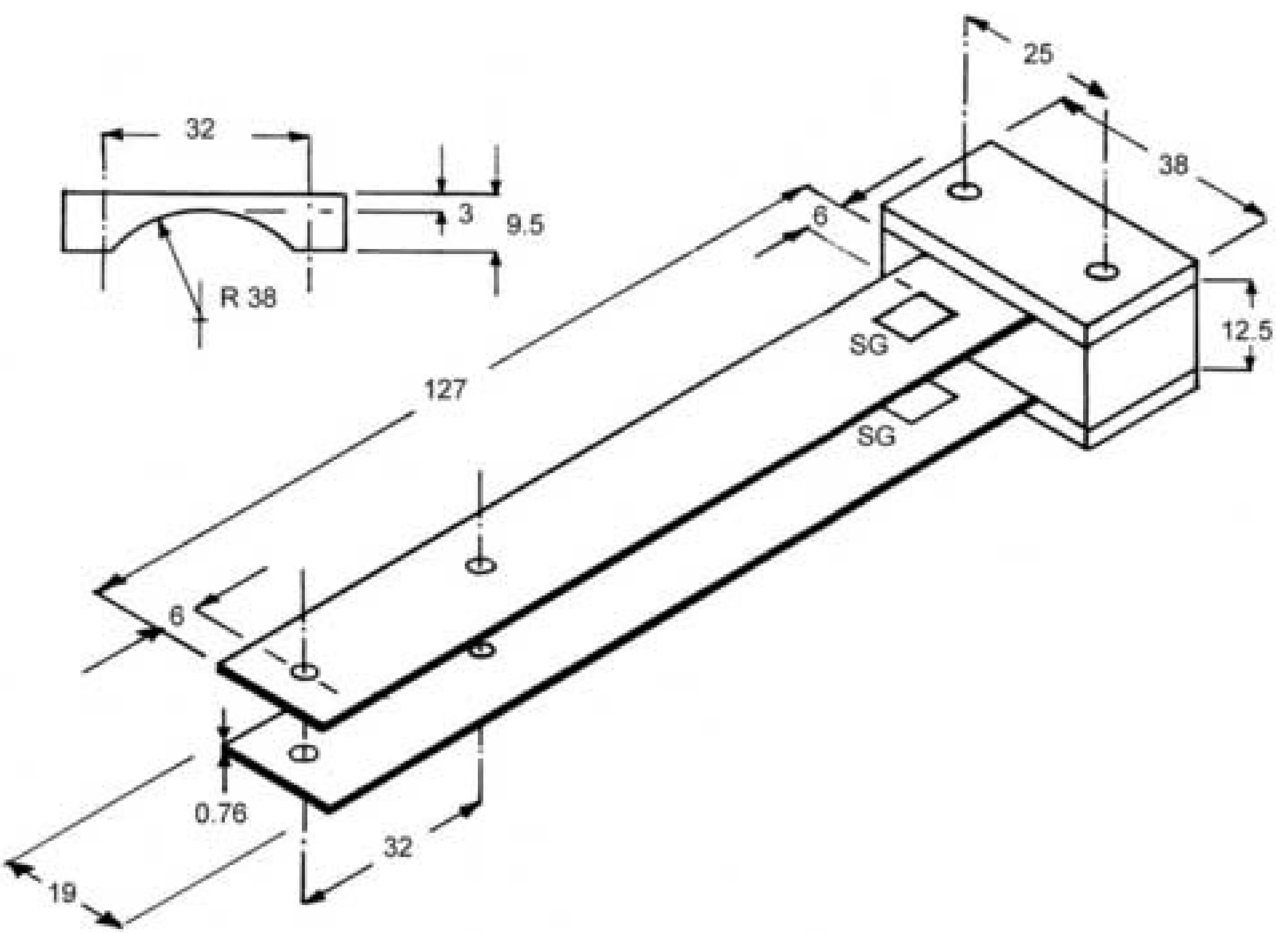

Figure7
Click here to download high resolution image

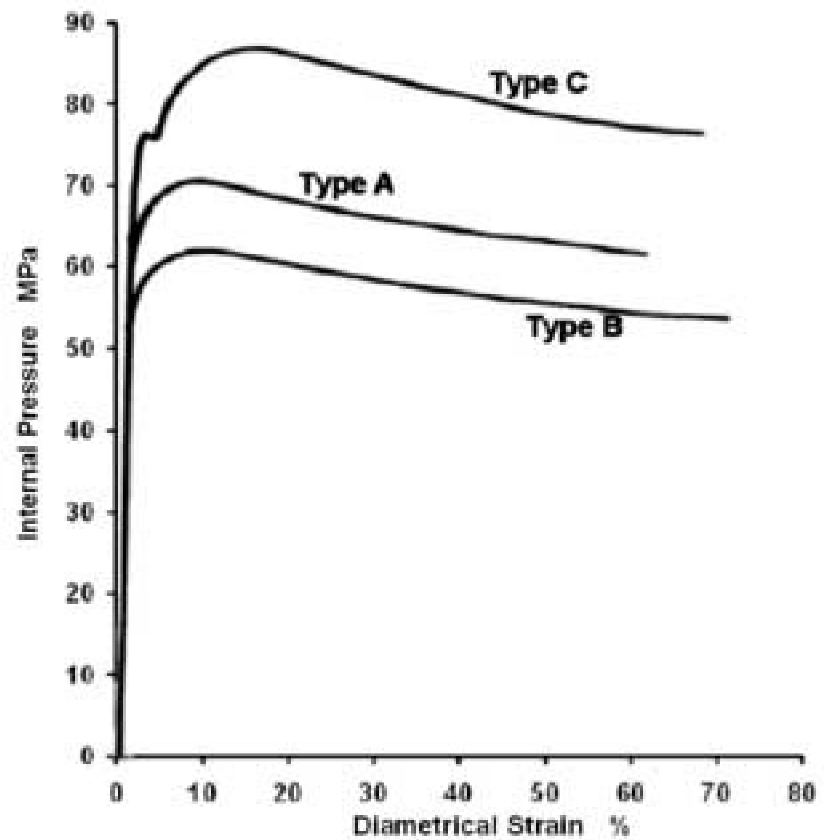

Figure8
Click here to download high resolution image

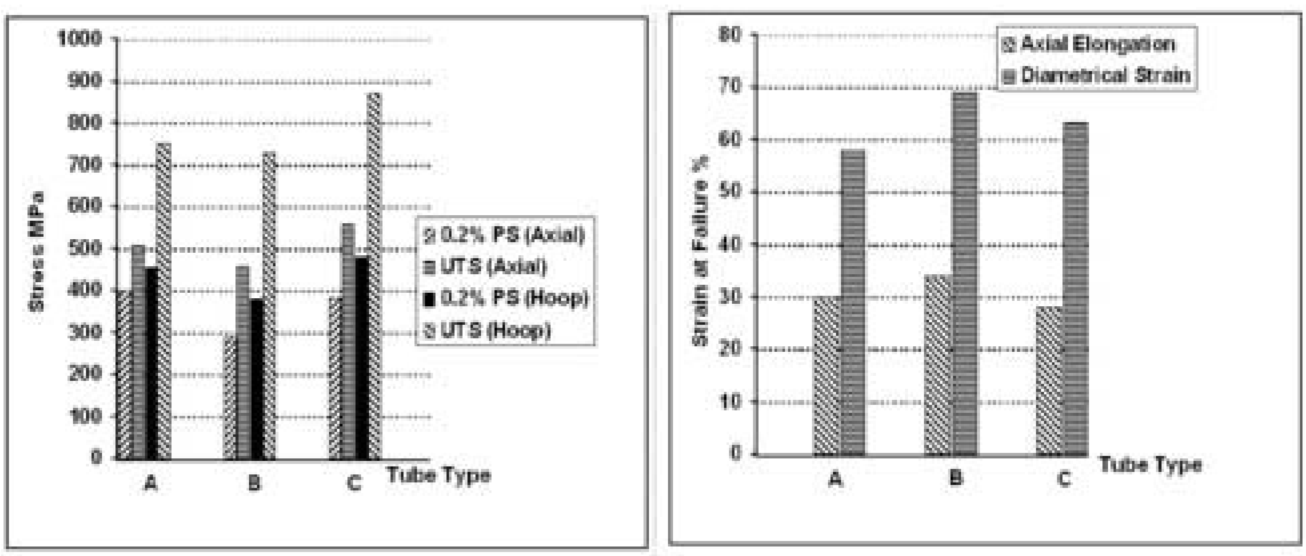

Figure9
Click here to download high resolution image

TABLE 1

Description of specimen tube types.

TUBE BATCH	INTERNAL DIAMETER 'a' mm	OUTSIDE DIAMETER 'b' mm	WALL THICKNESS 't' mm	OXYGEN CONTENT %
A (Vacuum annealed)	14.00	15.82	0.96	0.12
B	14.00	15.76	0.88	0.115
C	13.77	15.79	1.01	0.20

Table2

TABLE 2

Summary of results for tensile and circumferential loading tests (standard deviation in brackets).

TUBE BATCH	AXIAL LOADING CONFIGURATION			CIRCUMFERENTIAL LOADING CONFIGURATION		
	0.2% PROOF STRESS MPa	TENSILE STRENGTH MPa	ELONGATION %	0.2% PROOF STRESS MPa	CIRCUMFERENTIAL COMPONENT OF STRESS AT FAILURE MPa	DIAMETRICAL STRAIN %
A	400 (1.8)	506 (5.1)	30 (1.2)	454 (1.5)	748 (7.0)	58 (1.5)
B	289 (3.5)	455 (3.3)	34 (1.7)	379 (6.9)	727 (2.9)	69 (1.2)
C	383 (3.2)	559 (9.8)	28 (2.2)	478 (4.9)	870 (45.4)	63 (10.5)